4-2-2012

A FAP46 Mutant Provides New Insights into the Function and Assembly of the C1d Complex of the Ciliary Central Apparatus

Jason M. Brown
University of Massachusetts Medical School

Christen G. DiPetrillo
Dartmouth College

Elizabeth F. Smith
Dartmouth College

George B. Witman
University of Massachusetts Medical School

A FAP46 mutant provides new insights into the function and assembly of the C1d complex of the ciliary central apparatus

Jason M. Brown[1,*], Christen G. DiPetrillo[2,*], Elizabeth F. Smith[2,‡] and George B. Witman[1,‡]

[1]Department of Cell Biology, University of Massachusetts Medical School, Worcester, MA 01655, USA
[2]Department of Biological Sciences, Dartmouth College, Hanover, NH 03755, USA

*These authors contributed equally to this work
‡Authors for correspondence (elizabeth.f.smith@dartmouth.edu, george.witman@umassmed.edu)

Accepted 2 April 2012
Journal of Cell Science 125, 3904–3913

doi: 10.1242/jcs.107151

Summary

Virtually all motile eukaryotic cilia and flagella have a '9+2' axoneme in which nine doublet microtubules surround two singlet microtubules. Associated with the central pair of microtubules are protein complexes that form at least seven biochemically and structurally distinct central pair projections. Analysis of mutants lacking specific projections has indicated that each may play a unique role in the control of flagellar motility. One of these is the C1d projection previously shown to contain the proteins FAP54, FAP46, FAP74 and FAP221/Pcdp1, which exhibits Ca^{2+}-sensitive calmodulin binding. Here we report the isolation and characterization of a *Chlamydomonas reinhardtii* null mutant for FAP46. This mutant, *fap46-1*, lacks the C1d projection and has impaired motility, confirming the importance of this projection for normal flagellar movement. Those cells that are motile have severe defects in phototaxis and the photoshock response, underscoring a role for the C1d projection in Ca^{2+}-mediated flagellar behavior. The data also reveal for the first time that the C1d projection is involved in the control of interdoublet sliding velocity. Our studies further identify a novel C1d subunit that we term C1d-87, give new insight into relationships between the C1d subunits, and provide evidence for multiple sites of calmodulin interaction within the C1d projection. These results represent significant advances in our understanding of an important but little studied axonemal structure.

Key words: Pcdp1, Cilia, Dynein, *Chlamydomonas*, C1d-87

Introduction

Motile eukaryotic cilia and flagella are highly conserved organelles, virtually all of which are comprised of a '9+2' arrangement of microtubules where nine doublet microtubules with associated dynein arms and radial spokes surround a central pair of singlet microtubules and their associated projections. The central apparatus includes at least seven distinct protein projections and has been strongly implicated in regulating dynein-driven microtubule sliding to produce the complex waveforms characteristic of beating cilia and flagella (reviewed in Mitchell and Smith, 2009). Importantly, analyses of mutants which lack specific central pair projections have indicated that each complex may play a unique role in modulating motility (Adams et al., 1981; DiPetrillo and Smith, 2010; Dutcher et al., 1984; Lechtreck and Witman, 2007; Mitchell and Sale, 1999). The current challenge is to define the molecular mechanism by which this regulation is achieved.

DiPetrillo and Smith recently discovered a calcium-dependent calmodulin (CaM)-binding complex localized to the C1d projection of the central apparatus (DiPetrillo and Smith, 2010). They demonstrated that FAP54, FAP46, FAP74, and the CaM-binding protein FAP221/Pcdp1 are components of the C1d complex and that CaM binding to FAP221/Pcdp1 is calcium sensitive. Reduction of FAP74 levels using artificial microRNAs resulted in failure of C1d to assemble, with a concomitant reduction in the percentage of cells which effectively swam forward. The small percentage of FAP74 artificial microRNA (amiRNA) cells that were motile displayed a reduced beat frequency, defective waveform, and reduced ability to perform calcium-induced behaviors including waveform switching during photoshock and phototaxis (DiPetrillo and Smith, 2010; DiPetrillo and Smith, 2011). These severe motility defects indicate that C1d is crucial for wild-type (WT) beating.

Although these studies provided the first insights into the composition and function of the C1d projection, many questions remain. For example, does the C1d complex contain additional protein subunits? What are the precise protein–protein interactions among the C1d complex members and what is the functional consequence of these interactions? Which components are required for assembly/attachment of C1d to the central microtubule? How does the loss of C1d affect so many different motility parameters?

In this study we report the isolation and characterization of a null mutant for the *FAP46* gene. Structural, functional, and biochemical studies of the *fap46-1* mutant provide new insights into protein interactions and assembly of the C1d complex, identify a new C1d complex member, and reveal a requirement for FAP46 in the pathway that modulates the velocity of interdoublet sliding. These findings represent important steps towards defining a molecular mechanism for C1d assembly and function.

Journal of Cell Science

Results

Identification of a null mutant for FAP46

As part of an ongoing screen to identify new mutants with defects in flagellar assembly and function, we generated a collection of *Chlamydomonas reinhardtii* insertional mutants by transforming cells having WT motility (F2B4; see Materials and Methods) with a 1.7-kb fragment conferring resistance to hygromycin B (*aph7″*). Mutants with abnormal motility and mutants lacking flagella were maintained. To identify the genomic locations of the aph7″ inserts and the boundaries of any associated deletions, we amplified insert-flanking fragments using Restriction Enzyme Site Directed Amplification (RESDA) PCR (González-Ballester et al., 2005). For one strain, DNS11, *aph7″* was found to have inserted into the penultimate exon of the *FAP46* gene, accompanied by a genomic deletion of 9 bp (Fig. 1A). We named this allele *fap46-1*.

Cells of strain DNS11 assemble full-length flagella, but many cells are non-motile or swim with an aberrant twitchy movement (compare supplementary material Movie 1 with Movie 2). To determine whether *fap46-1* co-segregated with the swimming phenotype of DNS11, we backcrossed the mutant twice to WT strain 137c (Fig. 1B). Out of 376 colonies scored from both backcrosses, all mutant progeny were hygromycin resistant and all progeny wells that contained cells with only WT motility were sensitive to hygromycin, suggesting that the phenotype of DNS11 was caused by the *fap46-1* mutation. From among the mutant progeny of the second backcross, we selected mating type *plus* and *minus* lines for further analysis (supplementary material Movie 3). As no biochemical, structural, or behavioral differences were observed between the vegetative cells of these two strains, they hereafter will be referred to as *fap46-1 (mt+)* and *(mt−)*, respectively (mt, mating type), or simply *fap46-1*. Transformation of *fap46-1 (mt+)* with a cloned genomic fragment containing *FAP46* including 2045 bp upstream of the start codon and 941 bp downstream of the stop codon rescued the mutant phenotype (Fig. 1A,B; supplementary material Movie 4). The ~2 kb upstream of *FAP46* in the rescuing fragment included one small gene encoding ribosomal protein L30; sequencing indicated that this gene is not mutated in *fap46-1*. We also rescued *fap46-1 (mt+)* with a genomic *FAP46* construct modified to encode a C-terminal 3x-HA tag. The strains rescued with WT and HA-tagged versions of FAP46 will be referred to as *fap46-1::FAP46* and *fap46-1::FAP46-HA*, respectively (Fig. 1B).

Based on RESDA fragment sequencing, the *aph7″* insertion in *fap46-1* would cause a premature stop if the gene were fully translated. The result would be FAP46 protein lacking its C-terminal 167 amino acids (aa) but including 5 aa from the aph7″ gene. The predicted size of the WT protein is 290 kDa, whereas the predicted size of the truncated protein is 273 kDa. To further analyze *fap46-1* and rescued strains, we generated polyclonal antiserum by co-immunizing rabbits with N-terminal and C-terminal FAP46 peptides. Since these peptide sequences are both encoded upstream of the selectable marker insertion site (Fig. 1A), this antiserum should detect the truncated FAP46 protein if present. The antiserum detected a single predominant band of the expected size on western blots of WT whole flagella (Fig. 1C). This band was missing in *fap46-1* flagella and restored in *fap46-1::FAP46* and, with a slight upwards shift in mobility, in *fap46-1::FAP46-HA*. Importantly, no lower molecular weight bands indicating the presence of a truncated protein were detected by western blot in *fap46-1* or rescued strains (Fig. 1C). The combined data show that the aberrant swimming defect is caused by the *fap46-1* mutation, and that *fap46-1* is null for FAP46.

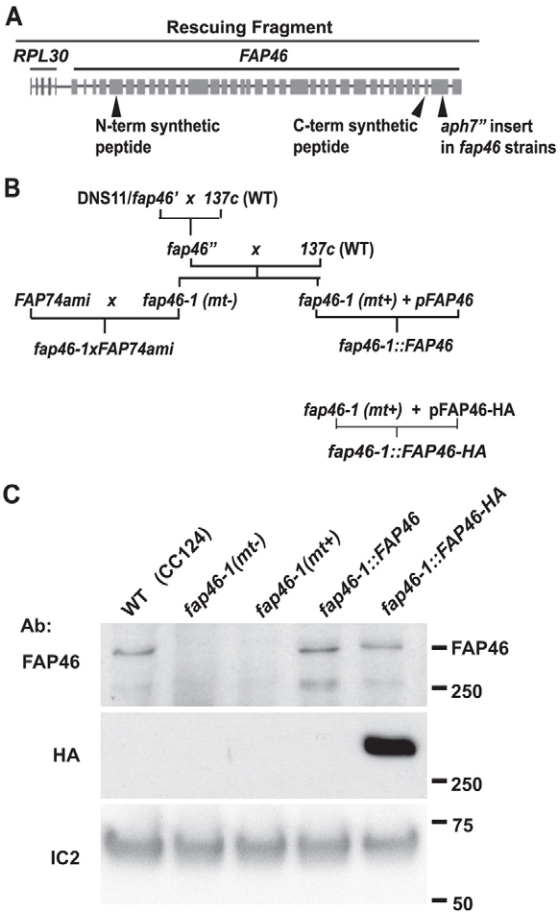

Fig. 1. *FAP46* gene, *fap46-1* null mutant strains, and *FAP46* rescued strains. (**A**) Diagram of *FAP46* gene and flanking regions; *FAP46* and *RPL30* exons are shown as grey boxes. Locations of aph7″ insert and synthetic peptide sequences used to make anti-FAP46 antibodies are indicated by arrowheads. The line above the genes represents the fragment used to rescue the *fap46-1* strain. (**B**) Pedigree charts showing generation of *fap46-1*, *fap46-1xFAP74ami*, *fap46-1::FAP46* and *fap46-1::FAP46-HA* strains used in this study. DNS11/*fap46'* is the *fap46-1* founder strain; *fap46″* is a progeny of a cross between DNS11 and the WT strain 137c. The *fap46-1 (mt+)* strain was transformed with a plasmid (pFAP46) containing the cloned WT *FAP46* gene or a plasmid (pFAP46-HA) containing a gene encoding HA-tagged FAP46, to generate the rescued strains *fap46-1::FAP46* or *fap46-1::FAP46-HA*, respectively. (**C**) Upper panel: western blot of flagella isolated from WT and the indicated *fap46-1* strains, probed with the anti-FAP46 antiserum. The antiserum recognizes a band of the expected size in WT that is missing in the *fap46-1 (mt−)* and *fap46-1 (mt+)* strains but restored in the *fap46-1::FAP46* rescued strain. FAP46–HA from the *fap46-1::FAP46-HA* strain migrates slightly slower than WT FAP46 due to the HA tag. Middle and lower panels: blots with loading equivalent to that of the blot in the upper panel were probed with anti-HA (middle panel) or an antibody to the outer dynein arm intermediate chain IC2 as a loading control (lower panel).

Axonemes lacking FAP46 do not assemble the C1d projection

FAP46 is a subunit of the C1d complex, which also contains FAP54, FAP74 and FAP221. To determine if assembly of the other subunits of the complex into the axoneme is impaired by

loss of FAP46, we probed western blots with antibodies to each of these proteins (Fig. 2A). Both flagella and isolated axonemes of the *fap46* mutant have reduced levels of FAP54, FAP74, and FAP221. All of these C1d complex subunits are restored to WT levels upon FAP46 rescue. Therefore, assembly of the intact complex into the axoneme is highly dependent on FAP46.

Previously, DiPetrillo and Smith reported that knockdown of FAP74 had little or no effect on the levels of flagellar FAP221 (DiPetrillo and Smith, 2010). That conclusion was based on western blots probed with anti-FAP221 antiserum which had not been affinity purified. Using that same antiserum in this study, we found that the predominant band identified in axonemes and axonemal extracts and of similar molecular weight to FAP221 is in fact comprised of more than one polypeptide, only one of which is FAP221 (supplementary material Fig. S1). Since affinity-purified anti-FAP221 antibody clearly showed a large reduction in FAP221 in *fap46-1* (Fig. 2A), we re-evaluated the levels of FAP221 in the FAP74 knockdown strain 1G11, hereafter referred to as *FAP74ami*. We also used the anti-FAP54 and anti-FAP46 antibodies which previously were not available to evaluate the levels of these proteins in *FAP74ami*. We found that knockdown of FAP74 reduced the levels of FAP54 and FAP46 (Fig. 2A). Moreover, FAP221 was no longer detectable in both flagella and axonemes, indicating a requirement for FAP74 in attachment of FAP221 to the axoneme. In *fap46-1xFAP74ami* combining *fap46-1* with FAP74 knockdown, the level of FAP54 was the same as in either single mutant, indicating that the effects of FAP46 and FAP74 loss are not additive for FAP54. As in *FAP74ami*, FAP221 was undetectable in the double mutant. Based on these combined results, we conclude that FAP46 and FAP74 are partially dependent upon each other for their assembly into the axoneme, that FAP54 is partially dependent on FAP46 and FAP74 for assembly, and that FAP221 is partially dependent on FAP46 and completely dependent on FAP74 for assembly.

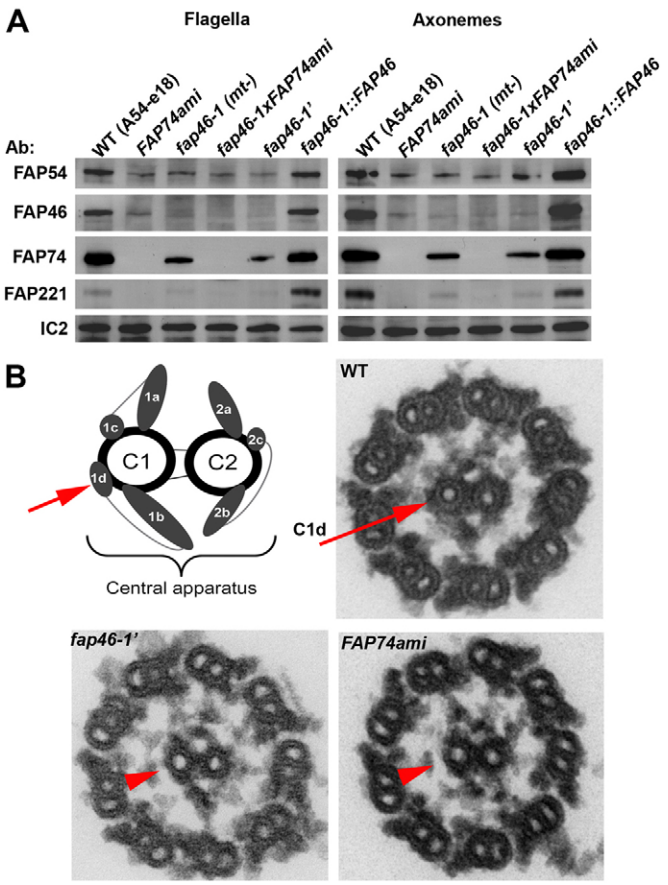

Fig. 2. Axonemes of *fap46-1* and *FAP74ami* retain different subunits, but both fail to assemble C1d. (**A**) Western blots of isolated flagella and axonemes from WT, mutant and rescued cells; *fap46-1'* is the *fap46-1* founder strain DNS11. FAP54, FAP46, FAP74 and FAP221 are C1d subunits. IC2 is an intermediate chain of the outer dynein arms and serves as a loading control. Affinity-purified antibody was used for the FAP221 blot. (**B**) Diagram showing the identities of the central pair projections; electron micrographs show axonemes from WT, the *fap46-1* founder strain DNS11 (*fap46-1'*), and the FAP74 knockdown strain (*FAP74ami*). All micrographs are oriented with the axoneme viewed proximal to distal; the C1 central microtubule in all images is to the left. The C1d projection in the diagram and in the electron micrograph of the WT axoneme is indicated by red arrows. The *fap46-1'* and *FAP74ami* axonemes lack the C1d density and the sheath connecting C1d to C1b (red arrowheads). Identical defects were observed for *fap46-1*. $n>50$ transverse sections resulting from two axoneme preparations for each strain.

To determine if the C1d central pair projection is altered in the *fap46-1* strain, we performed thin section electron microscopy. The C1d projection and sheath connecting C1d to C1b were not detectable in transverse sections of *fap46-1* axonemes, despite the presence of some FAP54, FAP74 and FAP221 (Fig. 2B). It is likely that the remaining C1d subunits are inadequate to create a structure readily detected by conventional electron microscopy. Note that *FAP74ami* also lacks the C1d projection and C1d to C1b sheath (Fig. 2B) (DiPetrillo and Smith, 2010).

FAP54 and FAP74 are associated as a sub-complex in the absence of FAP46

To determine if the C1d complex proteins that do assemble into *fap46-1* axonemes maintain their interactions with each other, we performed immunoprecipitation experiments using axonemal extracts prepared in the presence of 1 mM Ca^{2+} (Fig. 3A). As previously reported (DiPetrillo and Smith, 2010), the anti-FAP74 antibody co-precipitated FAP46, FAP54, FAP74 and FAP221 from WT axonemal extracts. Similar results were obtained with extracts from the *fap46-1* rescued strain. In contrast, the antibody co-precipitated only FAP54 and FAP74 from extracts from *fap46-1*. These results indicate that extracted FAP54 and FAP74 remain associated as a sub-complex in the absence of FAP46, but that FAP221 is either not associated with the sub-complex or bound so weakly that the association does not survive the immunoprecipitation.

C1d subunits without FAP221 are co-immunoprecipitated by anti-CaM antibodies

To further investigate C1d subunit associations in axonemal extracts of *fap46-1* and *FAP74ami*, we carried out immunoprecipitations using our anti-CaM antibody. In agreement with previous results (DiPetrillo and Smith, 2010), this anti-CaM antibody co-precipitated FAP46, FAP54, FAP74 and FAP221 from WT axonemal extracts (Fig. 3B). In contrast, the antibody co-precipitated FAP54 and FAP74 with no detectable FAP221 from the *fap46-1* extract; these results confirm that FAP54 and FAP74 form a sub-complex. The antibody co-precipitated FAP46 and FAP54 with no detectable FAP221 from axonemal extracts of *FAP74ami*; this result indicates that FAP46 and FAP54 remain associated as a sub-complex in the absence of

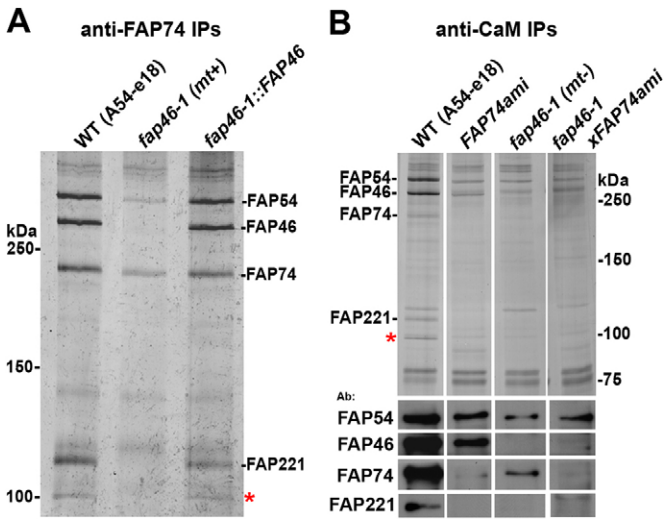

Fig. 3. FAP46, FAP54 and FAP74 form a sub-complex in extracts from C1d-defective axonemes. (**A**) Silver-stained gel of anti-FAP74 immunoprecipitations from high-Ca^{2+} NaCl extracts from WT, *fap46-1*, and *fap46-1::FAP46* axonemes. The immunoprecipitates from WT and the rescued strain *fap46-1::FAP46* are indistinguishable and contain the four previously described C1d subunits; that from *fap46-1* contains reduced amounts of FAP54 and FAP74 but no FAP46 or FAP221. (**B**) Silver-stained gel and corresponding western blots of anti-CaM immunoprecipitations from high-Ca^{2+} NaCl extracts from WT and mutant axonemes. FAP54 and FAP46 are co-precipitated from the extract of *FAP74ami* axonemes, FAP54 and FAP74 are co-precipitated from the *fap46-1* axonemal extract, and only FAP54 is precipitated from the *fap46-1xFAP74ami* axonemal extract. FAP221 is not detectable in the immunoprecipitates from any of the mutant extracts. Western blots for each antibody are from the same membrane and exposure; vertical white lines indicate that lanes were removed from between each sample. In both A and B, the red asterisk indicates a 100-kDa protein that is co-precipitated with C1d subunits from WT axonemal extracts but is not present in precipitates from C1d-defective mutants.

FAP74. Finally, the antibody precipitated FAP54 alone from axonemal extracts of the *fap46-1xFAP74ami* double mutant. These results suggest that FAP54 binds CaM.

The apparent absence of FAP221 from the *fap46-1* anti-CaM immunoprecipitate does not necessarily indicate that FAP221 cannot bind CaM in the context of the residual *fap46-1* C1d or by itself if it dissociated from the complex during the latter's extraction. The amount of FAP221 is so reduced in the mutant (Fig. 2A; supplementary material Fig. S1) that it simply may not have been detectable in our western blots.

Identification of an additional FAP46-binding partner with homology to human WDR93

In addition to the previously identified C1d proteins, the anti-FAP74 immunoprecipitate from the WT axonemal extract contained a prominent band at ~100 kDa that was absent from the *fap46-1* immunoprecipitate but present in the immunoprecipitate from the FAP46-rescued strain (Fig. 3A, asterisk). A similar band was present in the anti-CaM immunoprecipitate from WT axonemal extracts (Fig. 3B, asterisk), but was not observed in the anti-CaM immunoprecipitates from the mutant extracts. To investigate the possibility that this band represented an additional subunit of the C1d complex, we used an anti-HA antibody to immunoprecipitate FAP46-HA from axonemal extracts of the *fap46-1::FAP46-HA* strain (Fig. 4A). Six bands were observed specifically in the resulting immunoprecipitate; none of these was observed in anti-HA immunoprecipitates from WT (Fig. 4A) or *fap46-1* (result not shown) axonemal extracts. Four of these had mobilities corresponding to FAP46, FAP54, FAP74 and FAP221. Western blotting confirmed the identities of these four proteins in the immunoprecipitates from the *fap46-1::FAP46-HA* strain (Fig. 4A,B). The two additional bands had apparent molecular masses of 100 kDa and over 500 kDa (Fig. 4A, bands b and a, respectively); presumably, the 100-kDa protein is the same as that observed in the anti-FAP74 and anti-CaM immunoprecipitates. To determine the identities of the two unknown bands, they were excised from gels and analyzed by mass spectrometry.

The ~100-kDa protein in band b was identified as an uncharacterized protein (*C. reinhardtii* JGI v 4.0 protein ID 206529; GenBank EDP09774) of 813 aa with predicted mass of 87,230 Da and a pI of 7.60. Two peptides from this protein previously were found in the *Chlamydomonas* flagellar proteome (Pazour et al., 2005); importantly, the peptides originated from the 'extracted axoneme' fraction, which also included FAP46, FAP54, FAP74 and FAP221. As this protein is likely to be a novel subunit of the C1d complex we have named it C1d-87. C1d-87 has a central conserved WD-repeat domain likely to form a beta propeller structure involved in protein–protein interactions (Fig. 4C; supplementary material Fig. S2). C1d-87 also has a predicted CaM-binding domain from aa 180–190. Near its N-terminus, C1d-87 contains a 42-aa sequence that is 42.9% identical and 66.7% similar to an N-terminal region of the human WD-repeat protein WDR93 (Fig. 4C), which also is uncharacterized with regard to function. Despite the low sequence similarity over the rest of the length of these two proteins, human WDR93 and *C. reinhardtii* C1d-87 are reciprocal BLAST best hits. The conserved N-terminus appears to be found only in organisms with motile cilia. An alignment of sequences from 15 species with motile cilia indicates that the sequence DxLP(Q/M)P(Y/F)(R/K) is absolutely conserved (Fig. 4D; supplementary material Fig. S2). WDR93 also is predicted to contain two CaM-binding sites: one in the WD-repeat domain (as in C1d-87) and one near the C-terminus.

Mass spectrometry of the >500-kDa band revealed that it included all four previously identified C1d components as well as C1d-87. Given the relative mobility of this band, it likely represents C1d complexes that were not dissociated in SDS sample buffer. The sum of the predicted masses for these five proteins, 910 kDa, is consistent with this conclusion. Taken together, these data indicate that C1d-87 is a *bona fide* member of the C1d complex. That this complex remained intact through the harsh conditions of SDS-PAGE also indicates that FAP221 is tightly associated with the intact complex, in contrast to its weak or non-existent association with other members of the complex when FAP46 or FAP74 are missing.

Although C1d-87 is missing or reduced in the *fap46-1* lane in Fig. 3A and from the *fap46-1* and *FAP74ami* lanes in Fig. 3B, one cannot conclude from these immunoprecipitates that C1d-87 is missing from the residual C1d complex of the mutant axonemes. It is possible that C1d-87 is present *in vivo* but less tightly associated with the residual complex when FAP46 or FAP74 are missing, and hence lost from the residual complex during its extraction and immunoprecipitation. Assessment of the relative level of C1d-87 in the mutant axonemes will require an antibody to C1d-87, which is not yet available.

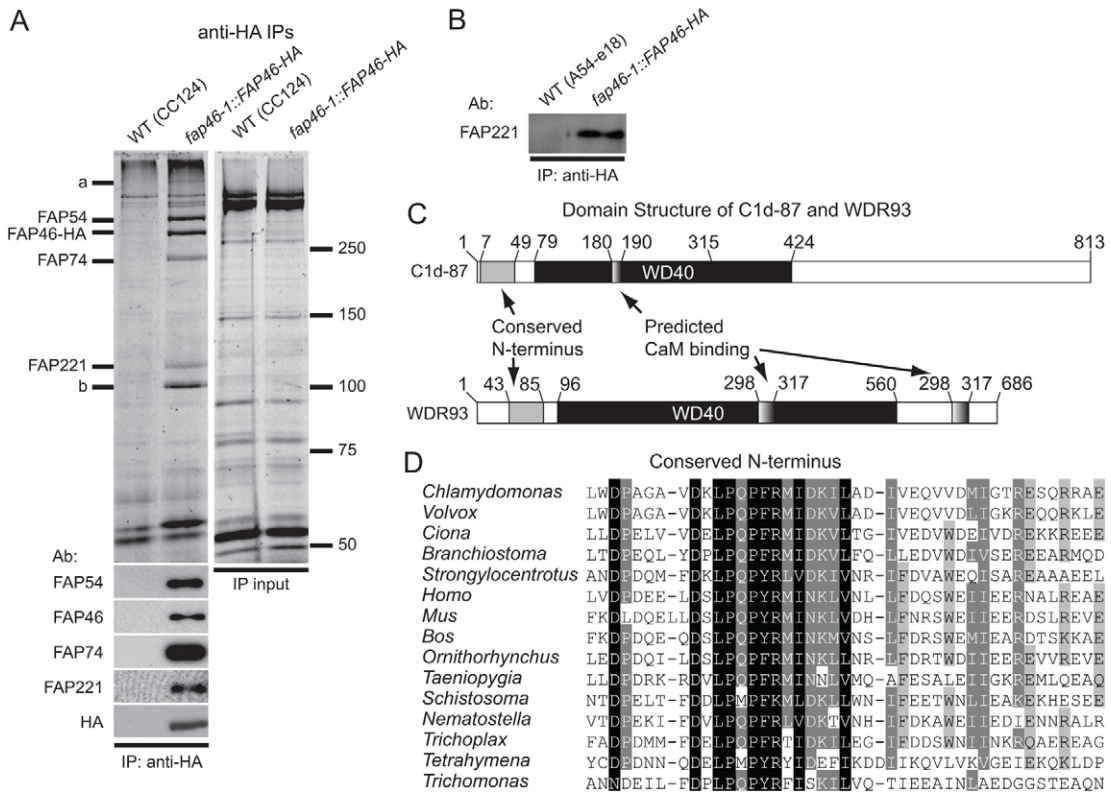

Fig. 4. A novel C1d subunit with a WD-repeat domain and an N-terminal domain conserved in organisms with motile cilia. (**A**) Upper panel: silver-stained gel of anti-HA immunoprecipitates from high-Ca^{2+} NaCl extracts from WT and FAP46-HA-rescued axonemes. Immunoprecipitation input lanes are on right. FAP46-HA, FAP54, FAP74 and FAP221 are specifically co-immunoprecipitated from the FAP46-HA rescued axonemal extract along with two unknown bands, a and b. Lower panel: Immunoblots of the same immunoprecipitates confirm that FAP46-HA, FAP54, FAP74 and FAP221 are specifically co-immunoprecipitated from the FAP46-HA-rescued axonemal extract. All blots were probed with antiserum. (**B**) Anti-HA-immunoprecipitate from a similar experiment probed with affinity-purified anti-FAP221 antibody, confirming that FAP221 is present in the immunoprecipitate from *fap46-1::FAP46-HA* axonemal extracts. (**C**) Domain maps of C1d-87, identified by mass spectrometry of band b from panel A, and its human homologue WDR93. The N-terminal domain is conserved only in organisms with motile cilia. (**D**) Sequence alignment illustrating the high degree of conservation of the N-terminal domain of C1d-87. The *C. reinhardtii* N-terminal region from aa 7–49 is aligned with highly similar regions of proteins from 14 other ciliated organisms ranging from protists to mammals. Protein sequences from which these amino acid sequences were taken are as follows [organism (accession information – all refer to NCBI reference sequences unless otherwise noted)]: *C. reinhardtii* (Joint Genome Institute *Chlamydomonas* v. 4.0 protein ID 206529); *Volvox carteri* (XP_002955486.1); *Ciona intestinalis* (XP_002126065.1); *Branchiostoma floridae* (XP_002601619.1); *Strongylocentrotus purpuratus* (XP_788085.2); *Homo sapiens* (NP_064597.1); *Mus musculus* (NP_001033016.1); *Bos taurus* (GenBank: AAI13295.1); *Ornithorhynchus anatinus* (XP_001509766.1); *Taeniopygia guttata* (XP_002197480); *Schistosoma mansoni* (XP_002577037.1); *Nematostella vectensis* (XP_001637625.1); *Trichoplax adhaerens* (XP_002110435.1); *Tetrahymena thermophila* (XP_001031667.1); *Trichomonas vaginalis* (XP_001312755.1).

fap46-1 and *FAP74ami* mutants have distinct motility phenotypes

Previously, DiPetrillo and Smith observed reductions in number of cells swimming, swimming velocity, and flagellar beat frequency in *FAP74ami* cells, the flagella of which almost completely lack FAP74 but retain considerable amounts of FAP46 (DiPetrillo and Smith, 2010). In contrast, *fap46-1* flagella completely lack FAP46 but retain considerable FAP74 (Fig. 2A). This difference presented an opportunity to assess the relative requirements for FAP46 and FAP74 in flagellar motility.

When observed by light microscopy, ~84% of WT cells were motile (Fig. 5A). In contrast, only 43% of *fap46-1* cells were motile, meaning that they are able to swim forward, albeit with slow, shaky progress; the remaining *fap46-1* cells had twitchy flagella that caused the cells to tumble in place, had flagella that were paralyzed, or were stuck to the microscope slide by their flagella. Swimming was even more impaired in *FAP74ami*, with only ~30% of cells motile. The double mutant combining *fap46-1* with FAP74 knockdown also exhibited ~30% motility, whereas motility was completely rescued in the *fap46-1::FAP46* strain. Supplementary material Movies 1–6 illustrate the swimming behavior in each of these strains. The results indicate that loss of FAP74 has a more severe effect on motility than loss of FAP46, and the effect is no more severe in the absence of both proteins.

A similar pattern was observed for forward swimming velocity, which was reduced to ~50% that of WT in *fap46-1* and to ~28% that of WT in *FAP74ami* (Fig. 5B). Again, the effect was no greater in the double mutant, and was rescued in the *fap46-1::FAP46* strain. This effect on swimming velocity is largely due to an effect on flagellar beat frequency, which was reduced to ~58% of the WT value in *fap46-1* and to less than 30% of WT in *FAP74ami* (Fig. 5D). The combined loss of FAP46 and FAP74 in the double mutant had no greater effect than the loss of FAP74 alone, and flagellar beat frequency was completely restored in the *fap46-1::FAP46* strain.

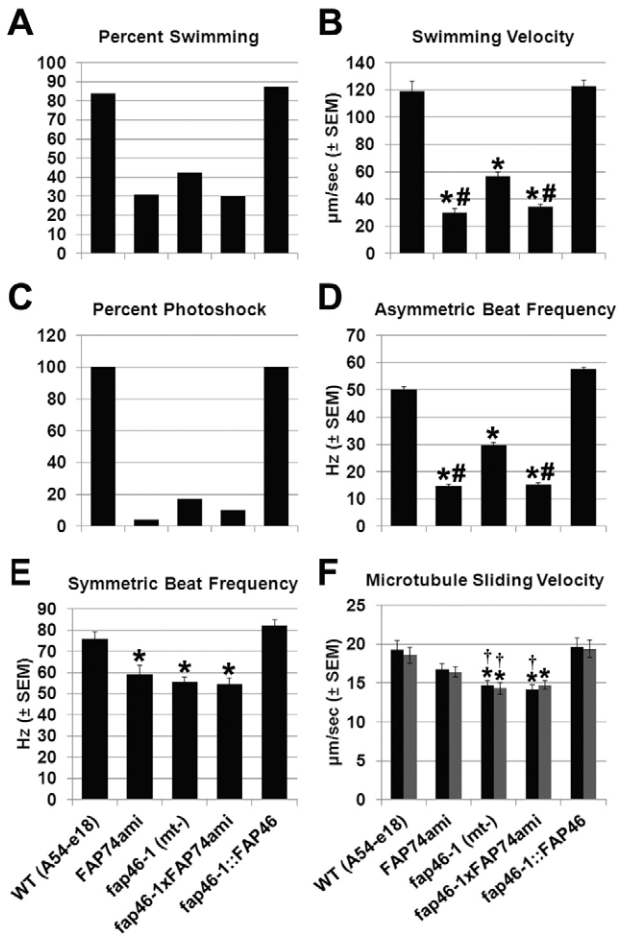

Fig. 5. Cells of *fap46-1* and *FAP74ami* strains have distinct motility phenotypes. (**A**) Percentage of cells swimming (n>130 for each); (**B**) average swimming velocity (n>40 for each); (**C**) percentage photoshock (values are percentages of the motile population; n>80 for each); (**D**) average asymmetric beat frequency (n>60 for each); (**E**) average symmetric beat frequency (n>8 for each) of WT, mutant and rescued strains. For each motility parameter, values for all strains were collected in the same experiment; the values for WT and *FAP74ami* strains were reported previously (DiPetrillo and Smith, 2011) and are included here for comparison. Where tested, asterisks (*) denote a significant difference (P<0.01) compared to WT and *fap46-1::FAP46*. Hash signs (#) denote a significant difference (P<0.01) from *fap46-1*. Error bars indicate ± s.e.m. (**F**) Average in vitro microtubule sliding velocity of WT and mutant axonemes treated with protease and ATP in either low (black bars) or high (grey bars) Ca^{2+} buffers. *Significant difference (P<0.01) from WT and *fap46-1::FAP46*; †significant difference (P<0.05) from *FAP74ami* (n>50 for each). Error bars indicate ± s.e.m.

Since the C1d complex binds to CaM in high calcium, we also compared the effect of loss of FAP46 versus FAP74 on two Ca^{2+}-mediated behaviors: phototaxis, in which cells swim toward or away from light; and photoshock, in which a sudden change in light intensity induces a momentary switching from the asymmetrical waveform used during forward swimming to the symmetrical waveform used during backward swimming, rapidly followed by a return to forward swimming (Bessen et al., 1980; Hyams and Borisy, 1978; Kamiya and Witman, 1984; Witman, 1993). Using a simple but sensitive photoaccumulation assay (Elam et al., 2011; King and Dutcher, 1997; VanderWaal et al., 2011), *FAP74ami* was found to be impaired in phototaxis as previously demonstrated using a more quantitative assay (DiPetrillo and Smith, 2011). Using the same simple assay, both *fap46-1* and *fap46-1*x*FAP74ami* were severely impaired in the ability to phototax; only the FAP46-rescued strain exhibited WT phototaxis. Photoshock also was severely impaired in all mutant strains (Fig. 5C): 100% of WT cells exhibited photoshock upon light step-up, whereas only 17%, 4%, and 10% of *fap46-1*, *FAP74ami* and *fap46-1xFAP74ami* cells, respectively, underwent photoshock. Photoshock was completely restored in the FAP46-rescued strain. Therefore, the C1d complex is very important for phototactic steering and switching between asymmetrical and symmetrical flagellar waveforms.

Although only a low percentage of mutant cells underwent photoshock, for those that did we measured the beat frequency of the symmetrically beating flagella. Symmetrical beat frequency was reduced to ~72% of the WT value in both *fap46-1* and *FAP74ami*; interestingly, this reduction was much less than that observed for the asymmetrical beat frequency (58% and 30% of WT, respectively; cf. Fig. 5D,E). Combining *fap46-1* and FAP74 knockdown had no further effect, and symmetrical beat frequency was restored to WT values in the FAP46-rescued strain.

Flagellar motility defects can be due to defects in the rate of dynein-driven microtubule sliding, defects in coordinating dynein activity among doublet microtubules, or both. To distinguish between these possibilities for *fap46-1* axonemes, we performed *in vitro* microtubule-sliding assays that assess microtubule sliding uncoupled from axonemal bending (Fig. 5F). Loss of FAP46 resulted in a significant reduction in microtubule-sliding velocity from ~18 μm/s in WT to ~14 μm/s in *fap46-1*; similar differences were observed regardless of whether the assay was carried out in high or low Ca^{2+} buffer. In contrast, and as previously shown (DiPetrillo and Smith, 2011), the difference in microtubule sliding velocities between *FAP74ami* and WT was not statistically significant. The microtubule-sliding velocities for *fap46-1* in both high- and low-Ca^{2+} buffers also were modestly but significantly slower than those for *FAP74ami*. In the double mutant combining *fap46-1* with FAP74 knockdown, microtubule-sliding velocities were similar to those observed in the *fap46-1* single mutant. Therefore, microtubule-sliding velocities are significantly decreased in *fap46-1* but not in *FAP74ami* compared to WT. In contrast, the reduction in swimming velocity and asymmetrical beat frequency is greater in *FAP74ami* than in *fap46-1*. These results suggest that the different C1d subunits remaining in *fap46-1* and *FAP74ami* lead to differential effects on dynein activity and coordination.

Discussion

DiPetrillo and Smith showed that the C1d projection of the *Chlamydomonas* flagellar central apparatus contains at least four proteins: FAP46, FAP54, FAP74 and FAP221, which in mammals is called Pcdp1 (Lee et al., 2008; DiPetrillo and Smith, 2010). Using amiRNA to reduce expression of FAP74, DiPetrillo and Smith also demonstrated that the C1d projection is essential for WT motility. In the current work, the identification of a mutant null for FAP46 confirmed the latter result and led to the discovery of another C1d complex protein that we have named C1d-87. The data presented here also underscore the importance of the C1d complex for Ca^{2+}-mediated behavioral responses (DiPetrillo and Smith, 2011), provide new information on the relationships between subunits within this central pair

projection, and begin to establish specific protein interactions required for C1d complex assembly. The results also reveal that motility parameters are affected differently by loss of different C1d subunits: loss of FAP74 is specifically associated with defects in coordination of interdoublet sliding (DiPetrillo and Smith, 2011), whereas loss of FAP46 is specifically associated with a decrease in interdoublet sliding velocity. These results represent significant steps towards understanding the composition, assembly, and function of this important central pair projection.

Interactions among C1d subunits

In the absence of FAP46, the levels of FAP54, FAP74 and FAP221 in the axoneme are greatly reduced; when FAP74 is knocked down, the levels of FAP46 and FAP54 in the axoneme are greatly reduced and FAP221 is no longer detectable (Fig. 2A, Fig. 6). These results indicate that FAP46 and FAP74 are partially dependent upon each other for normal assembly into the axoneme and that FAP54 is partially dependent upon both of these proteins for its assembly into the axoneme. FAP221 appears to be completely dependent upon FAP74 for its assembly into the axoneme. Moreover, both anti-FAP74 and anti-CaM antibodies co-precipitate FAP54 and FAP74 with no detectable FAP221 from extracts of *fap46-1* axonemes, and the anti-CaM antibody co-precipitates FAP46 and FAP54 from extracts of *FAP74ami* axonemes (Fig. 3A,B, Fig. 6). Therefore, FAP54 associates with FAP74 even in the absence of FAP46, and with FAP46 even in the absence of FAP74. These results indicate that FAP46, FAP54 and FAP74 interact as a potentially heterotrimeric sub-complex within the C1d projection. Some FAP54 is assembled into axonemes of the double mutant lacking FAP46, FAP74, and FAP221 (Fig. 2A, Fig. 3B), suggesting that FAP54 binds to the C1 microtubule either directly or through an as-yet unidentified intermediary.

Although FAP221 is clearly part of the C1d complex, as indicated by its co-precipitation with other subunits of the complex from extracts of WT axonemes, it no longer co-precipitates with the remaining subunits of the FAP46/FAP54/FAP74 sub-complex when FAP46 is missing and it is absent from axonemes when FAP74 is absent (Fig. 3A,B, Fig. 6). Therefore, the association of FAP221 with this sub-complex requires FAP74 and is somewhat dependent on the presence of FAP46. FAP221 may also be directly associated with C1d-87. C1d-87 is clearly present with FAP221 in anti-FAP74 and anti-CaM immunoprecipitates from WT axonemal extracts (Fig. 3A,B), and in anti-HA immunoprecipitates from the FAP46-HA-rescued strain (Fig. 4A). However, like FAP221, it is absent or greatly reduced in immunoprecipitates from axonemal extracts of *fap46-1* or *FAP74ami*. These observations raise the possibility that the assembly of C1d-87 is dependent on that of FAP221, and vice versa.

CaM interactions with C1d subunits

FAP221 was previously shown to contain a CaM-binding site, is the only one of the known C1d subunits that binds CaM in a CaM-overlay assay, and is presumed to be responsible for the association of CaM with the C1d complex and for immunoprecipitation of the complex by the anti-CaM antibody (DiPetrillo and Smith, 2010). As noted above, FAP221 is greatly reduced or absent, respectively, from axonemes of *fap46-1* and *FAP74ami*. It was therefore unexpected that anti-CaM antibodies immunoprecipitated FAP54 and FAP74 from extracts of *fap46-1*

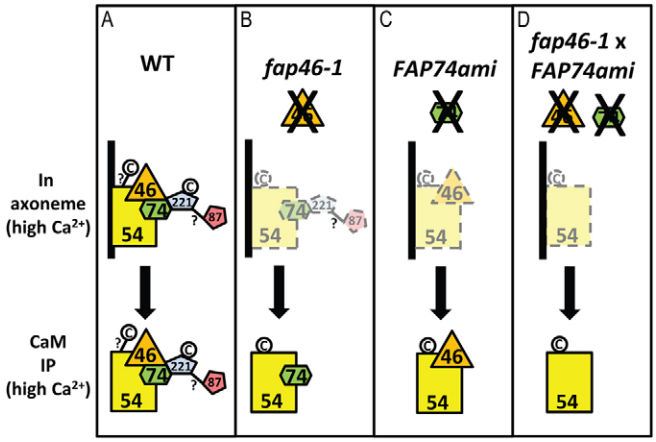

Fig. 6. Model for C1d subunit interactions. Predicted interactions between C1d subunits in WT and *fap46-1*, *FAP74ami* and *fap46-1xFAP74ami* mutant strains in the presence of high Ca^{2+}. 54, FAP54; 46, FAP46; 74, FAP74; 221, FAP221; 87, C1d-87; C, CaM. The thick vertical lines represent C1 microtubules. Faded shading with dashed outlines indicate decreased axonemal content relative to WT. Arrows represent 0.6 M NaCl extraction and dialysis with NaLow. (**A**) On WT axonemes, FAP46, FAP54, FAP74, FAP221, C1d-87 and CaM form a complex that can be extracted with 0.6 M NaCl and immunoprecipitated from the extract by an anti-CaM antibody. The direct interaction between FAP221 and C1d-87 is speculative, as indicated with a question mark. FAP54 may or may not bind CaM in WT cells, as indicated by a second question mark. (**B**) In *fap46-1* axonemes, FAP54, FAP74 and FAP221 are present in reduced amounts and anti-CaM co-immunoprecipitation of FAP54 and FAP74 without FAP221 suggests formation of a FAP54/FAP74/CaM sub-complex and partial requirement of FAP46 for FAP221 binding to C1d. Although C1d-87 is shown, it is not yet known if this subunit is part of the residual C1d complex in *fap46-1*. (**C**) In *FAP74ami* axonemes, FAP54 and FAP46 are present in reduced amounts; absence of FAP221 indicates that FAP74 is required for FAP221 binding to C1d. Anti-CaM co-immunoprecipitation of FAP54 and FAP46 suggests that FAP46 is included with FAP54, FAP74 and CaM in a C1d sub-complex. (**D**) In *fap46-1xFAP74ami*, FAP54 is present in reduced amounts. Axonemal binding of FAP54 in the absence of other C1d proteins suggests direct binding of FAP54 to the C1 microtubule, and immunoprecipitation of FAP54 by anti-CaM suggests direct binding of CaM to FAP54.

and immunoprecipitated FAP46 and FAP54 from extracts of *FAP74ami*; FAP221 was not detectable in these precipitates. The anti-CaM antibodies precipitated FAP54 alone from axonemal extracts of the double mutant combining *fap46-1* with FAP74 knockdown; again, FAP221 was not detectable in the precipitate. These results suggest that FAP54 interacts with CaM. Indeed, analysis of the FAP54 sequence using online tools available at The Calmodulin Target Database (http://calcium.uhnres.utoronto.ca/ctdb/ctdb/sequence.html) identified a high-scoring putative CaM-binding site at aa 1701–1706 and a lower scoring potential IQ motif at aa 2958–2972. Although DiPetrillo and Smith did not observe CaM binding to FAP54 in gel-overlay assays, it is possible that FAP54 binds CaM only in its native form (DiPetrillo and Smith, 2010).

The newly identified C1d-interacting protein C1d-87 also has a predicted CaM-binding domain (Fig. 4C). However, little if any C1d-87 is present in the anti-CaM precipitations from *fap46-1*, *FAP74ami*, or the double mutant combining *fap46-1* and FAP74 knockdown (Fig. 3B), so C1d-87, if it binds CaM, cannot be responsible for the anti-CaM precipitation of the remaining

subunits of the C1d complex in the absence of FAP221. Nevertheless, it is of interest that three subunits of the C1d projection bind or are predicted to bind CaM. This is consistent with the severe defect in Ca^{2+}-mediated photobehaviors in cells lacking this projection.

Generation and regulation of motility

In axonemes of *fap46-1*, FAP46 is absent and FAP74 present, albeit in reduced amounts; conversely, in axonemes of *FAP74ami*, FAP74 is almost completely gone and FAP46 present, albeit in reduced amounts. Therefore, by comparing the relative effects on various parameters of motility in these two strains, we are able to gain insight into the specific requirements for FAP46 and FAP74 in the generation and control of flagellar movement. In *fap46-1*, the decrease in swimming velocity and asymmetrical beat frequency are not as large as in *FAP74ami*, yet the effect on microtubule-sliding velocity is much greater. This correlation between loss of FAP46 and reduced sliding velocity suggests either that FAP46 is specifically involved in the control of sliding velocity, or alternatively, that the absence of FAP46 alters the arrangement of the remaining members of the C1d complex in a manner that specifically affects sliding. In contrast, in *FAP74ami* a large decrease in swimming velocity is accompanied by a large decrease in asymmetrical beat frequency, but without a corresponding decrease in microtubule-sliding velocity. Since swimming velocity is determined by both the velocity of microtubule sliding and the coordination of this sliding to produce productive waveforms, this result suggests that FAP74 has a key role in the latter. Supporting this conclusion, the pattern of microtubule sliding in disintegrated axonemes of *FAP74ami* is abnormal (DiPetrillo and Smith, 2011). Our results demonstrate for the first time that the C1d projection is important both for regulating the rate of interdoublet sliding and for coordinating this sliding, two parameters that are intimately linked and must be controlled in concert to produce efficient and effective flagellar beating.

The loss of FAP46 severely affected Ca^{2+}-mediated photobehaviors: phototaxis was completely eliminated, and the percent of cells that underwent photoshock was reduced to only ~17% of WT values (Fig. 5C). This confirms that the nearly identical effect previously reported for knockdown of FAP74 (DiPetrillo and Smith, 2011) is due to loss of the C1d projection rather than off-target effects of the artificial microRNA procedure. It is likely that FAP46 and FAP74 exert their effects via interaction of C1d with the radial spoke heads, with information about this interaction relayed instantaneously by the radial spokes to the dynein regulatory complex and the dynein arms. Given that the association of CaM with FAP221 is calcium dependent, our working hypothesis is that Ca^{2+}–CaM interaction with FAP221 and possibly other subunits of the C1d complex alters the conformation of subunits within C1d in such a way that the association of the C1d projection with the radial spoke head is changed. This hypothesis might be tested by high-resolution cryo-electron microscopy of the C1d projection in the presence and absence of Ca^{2+}–CaM, or by examining C1d-radial spoke head interaction *in vitro* in the presence and absence of Ca^{2+}–CaM. It also may be relevant that, in sea urchin sperm, recent studies indicate that it is the rate of Ca^{2+} influx into the flagellum rather than the final intraflagellar Ca^{2+} concentration that is responsible for altered flagellar waveform during chemotaxis (Alvarez et al., 2012). A ‘chemical differentiator model’ was proposed to explain this phenomenon; this model depends on two proteins or two domains within one protein with different binding affinities for Ca^{2+} and opposite effects on flagellar beat parameters. If *Chlamydomonas* flagella similarly respond to the rate of change of Ca^{2+} rather than absolute Ca^{2+} concentration, it is plausible that differences in affinity for Ca^{2+}–CaM between different C1d subunits or between different proteins of C1d versus C1a (see below) could satisfy the requirements of the chemical differentiator model.

The effects of disruption of C1d function are in marked contrast to the phenotypes that result from perturbation of other central pair projections. For example, loss of the C1b projection in the *cpc1* mutant reduces flagellar beat frequency but has no effect on phototaxis or the photoshock response (Mitchell and Sale, 1999). Loss of the C1a projection in *pf6* blocks motility (Rupp et al., 2001), precluding analysis of a specific effect on phototaxis and photoshock. Knockdown of hydin causes specific loss of the C2b projection with the consequence that most cells are paralyzed with only a few twitching or swimming in place (Lechtreck and Witman, 2007), again preventing assay of effect on phototaxis and photoshock. The complete absence of the central pair apparatus that occurs in some other mutants also results in complete paralysis (Witman et al., 1978). Our results and those of DiPetrillo and Smith (DiPetrillo and Smith, 2010; DiPetrillo and Smith, 2011) indicate that although the C1d projection is not as essential for forward motility as are the C1a and C2b projections, it is very important for phototactic steering and switching from an asymmetric to symmetric waveform, both of which are mediated by Ca^{2+}. Thus, it is not surprising that the C1d projection contains at least one and possibly more subunits that bind CaM in a Ca^{2+}-dependent manner. Inasmuch as the C1a projection also has a CaM-binding subunit (Wargo et al., 2005), we propose that the C1 microtubule is a central hub for the Ca^{2+}-mediated control of flagellar motility.

Materials and Methods

Strains and cell culture

Chlamydomonas reinhardtii strain A54-e18 (*nit1-1*, *ac17*, *sr1*, *mt+*) has WT motility and was obtained from Paul Lefebvre (University of Minnesota, St Paul, MN). The WT strains 137c (*mt−*) (CC124), 137c (*mt+*) (CC125), and the central pair-less strain *pf18* were obtained from the *Chlamydomonas* Genetics Center (University of Minnesota, MN). *FAP74ami* transformant 1G11 was generated as described previously (DiPetrillo and Smith, 2010). For the experiments in Figs 2, 3 and 5, cells were grown in constant light in TAP media (Gorman and Levine, 1965). For immunoprecipitation of FAP46-HA and the western blot in Fig. 1C, cells were grown in M medium on a light/dark cycle of 14/10 h (Witman, 1986).

The *fap46-1* mutant strain was generated in a dual screen designed to isolate novel motility mutants and mutants involved in regulation of genes encoding flagellar proteins (J.M.B. and G.B.W., unpublished data). The parental strain, F2B4, had WT motility and contained a reporter construct leading to the induction of luciferase expression following deflagellation. The insertional mutant DNS11 was isolated as described below and was backcrossed twice to WT to generate strains *fap46-1 (mt−)* and *fap46-1 (mt+)*. The luciferase construct was not present in the progeny of the second backcross (result not shown) and therefore did not contribute to the reported phenotype. The double mutant strain 11A2 (*fap46-1xFAP74ami*) was selected from a nonparental ditype tetrad and confirmed by western blot. See Fig. 1 for a diagram of these crosses.

Insertional mutagenesis and identification of insert boundaries

To generate insertional mutants, strain F2B4 was transformed with the 1.7 kb HindIII fragment of pHyg3 (Berthold et al., 2002) and selected with 10 µg/ml hygromycin B on TAP agar plates. Resistant clones were screened for lack of WT motility. To identify the genomic sequences surrounding pHyg3 insertion sites in these mutants, genomic DNA was subjected to RESDA PCR (González-Ballester et al., 2005). Primers used for the first-round reactions were one pHyg3-specific primer, either UP2 or DP4 (Matsuo et al., 2008), along with one degenerate primer, either degAluI, degPstI, degSacI, or degTaqI (González-Ballester et al., 2005). Primers used in the second round reaction were either UP1 or DP3 (Matsuo et al., 2008) along with Q0 (González-Ballester et al., 2005). PCR products were excised

from gels and subjected to direct sequencing using primer UPS or DPS (Matsuo et al., 2008).

FAP46 gene cloning, rescue, and HA tagging

To construct the WT *FAP46* rescue plasmid, a 17.5-kb HindIII–EcoRI fragment containing the complete genomic sequence was subcloned from the Bacterial Artificial Chromosome clone 27L02 (Clemson University Genomics Institute) into pNEB193 (New England Biolabs). A cassette conferring resistance to phleomycin (Stevens et al., 1996) was inserted into the HindIII site to generate the rescue plasmid, pFAP46. To test for the ability of WT *FAP46* to rescue the *fap46-1* phenotype, *fap46-1 (mt+)* was transformed by electroporation with pFAP46. Electroporation conditions were modified from Pollock et al., (Pollock et al., 2004) as follows: Cells grown in M medium were harvested and transferred to 1/3 volume of TAP medium for 4 hr. The cells were then concentrated to $2X10^8$ cells ml^{-1} in TAP + 40 mM sucrose; 80 µl of cells + 1 µg EcoRI-linearized pFAP46 were pulsed once in a 0.1 cm cuvette with an ECM 600 electroporator (BTX) at 200 V (2000 V cm^{-1}), 1000 µF, and 13 Ω. Cells were allowed to recover overnight in 10 ml TAP + 40 mM sucrose prior to plating on selective medium. One of the rescued strains, *fap46-1::FAP46*, was used for further characterization of the rescued phenotype.

To generate a construct to express FAP46 with a 3x-HA tag on its C-terminus, two fragments were amplified from pFAP46 using Herculase-II fusion DNA polymerase (Agilent) adding BamHI and AvrII restriction sites for HA-tag insertion upstream of the *FAP46* stop codon. The two fragments were subsequently cloned into pGEM-Teasy (Promega). The resulting plasmid (pFAP46Cterm) was digested with BamHI and AvrII and the 3x-HA tag from pKL3 (Lechtreck and Witman, 2007) was inserted. Finally, the HA-tagged 1.8-kb BsaBI–BstEII fragment was inserted into pFAP46, replacing the corresponding untagged BsaBI–BstEII fragment, to generate pFAP46–HA. To generate an HA-tagged rescued strain, *fap46-1 (mt+)* was transformed by electroporation with pFAP46–HA. Phleomycin-resistant clones that recovered WT motility were further screened for FAP46–HA by western blotting. FAP46HA2.2 (*fap46-1::FAP46-HA*) was selected from among the HA-positive strains for further analysis.

Axoneme isolation, protein extraction, and immunoprecipitation

Flagella and axonemes were isolated and extracted as previously described (DiPetrillo and Smith, 2010) using the dibucaine method (Witman, 1986). NaCl extracts using 0.6 M NaCl were prepared for all experiments utilizing axonemal extracts. For experiments performed in the presence of high Ca^{2+}, NaLow and NaHigh were both modified to contain 1.0 mM $CaCl_2$ and EDTA was omitted. Anti-calmodulin and anti-FAP74 immunoprecipitations were performed as described previously (DiPetrillo and Smith, 2010). Anti-HA immunoprecipitations were carried out in high Ca^{2+} and 0.5% polyethylene glycol 20,000 was added to both NaLow and NaHigh during axoneme isolation, 0.6 M NaCl extraction, and dialysis. 300 µg of dialyzed NaCl extract was precleared with pre-rinsed protein G magnetic beads (Invitrogen Dynal) for 30 min at 4℃. The pre-cleared extract was combined with pre-rinsed beads from 50 µl slurry and 5 µg of chromatin immunoprecipitation grade rabbit anti-HA antibody (Abcam) and incubated at 4℃ overnight. After four washes, bound proteins were eluted for 20 min at room temperature with 60 µl of 1 mg/ml HA peptide in 167 mM NaCl, 10 mM Tris-HCl, pH 7.5, 0.05% Tween 20, 1 mM $CaCl_2$ and 0.25× plant protease inhibitor cocktail (Sigma). Samples were either analyzed directly by SDS-PAGE or were precipitated with methanol and chloroform (Wessel and Flügge, 1984) to concentrate proteins prior to SDS-PAGE.

Construction of expression vectors, antibody production, and affinity purification

Polyclonal antibodies for FAP54 were generated in rabbits against bacterially expressed proteins. Reverse transcriptase-PCR was used to generate cDNA encoding amino acids 29–387 (N-terminal) and 2902–3129 (C-terminal). The amplified PCR product was ligated into the PCR2.1 vector using the TOPO-TA cloning kit (Invitrogen, Carlsbad, CA). PCR fragments were then cloned into the pET30C or pET30A expression vector, respectively (Novagen, Madison, WI). Orientation and reading frame were confirmed by DNA sequencing. The construct was transformed into BL21 (DE3) pLysS cells (Novagen) and expression was induced using 2 mM IPTG. Protein was purified on a Ni^{2+}-resin column according to the manufacturer's instructions (Novagen). Peak fractions were dialyzed against 2.0 M urea in PBS, fixed with SDS sample buffer, and subjected to SDS-PAGE. Protein bands were excised from Coomassie-stained gels and used for polyclonal antibody production in rabbits. Rabbits were co-injected twice with 300 µg of each protein per injection. Antibody production was conducted by Spring Valley Laboratories (Woodbine, MD).

Polyclonal antibodies for FAP46 were generated in rabbits against synthetic peptides corresponding to amino acids 372–386 (N-terminus) and 2552–2566 (C-terminus). Each synthetic peptide had a cysteine added to the C-terminal end and was conjugated to keyhole limpet hemocyanin before being used for antibody production by Spring Valley Labs (Woodbine, MD). The N-terminal and C-terminal synthetic peptides were co-injected into rabbits for antibody production.

Anti-FAP74 and anti-FAP221 antibody production was described previously (DiPetrillo and Smith, 2010). To affinity purify FAP221 antibody, 800 µg of the bacterially expressed FAP221 fragment used to generate the antibody was separated by SDS-PAGE and transferred to nitrocellulose. After staining the membrane with Ponceau S (Fisher Scientific) for 1 min, the protein strip was trimmed from the membrane and washed in TBST (150 mM NaCl, 50 mM Tris-HCl, pH 7.4, 0.1% Tween 20, 0.5 mM EDTA, 0.2% sodium azide) to remove the Ponceau S. The membrane strip was blocked in TBST + 5% milk for 1 hour, folded to fit inside a 2-ml tube containing FAP221 anti-serum, and incubated for 16 hours at 4℃. After washing the strip with TBST, the antibody was eluted with 3 ml of 0.1 M glycine pH 2.8 for 4 min and then 300 µl of 0.1 M Tris-HCl pH 8 was immediately added. Finally the affinity-purified antibody was dialyzed into phosphate-buffered saline.

Gel electrophoresis, silver staining and western blots

Prior to silver staining or western blotting, protein samples were subjected to SDS-PAGE using either 5% or 6% polyacrylamide gels. Silver staining was performed as previously described (Wargo et al., 2005) or using the Silver Stain Plus kit (Bio-Rad) according to the manufacturer's instructions. Western blots were prepared by transferring proteins from gels to polyvinylidene difluoride (Immobilon P; Millipore). Serum antibodies were used for probing western blots at 1:1000 (FAP46, FAP54 and FAP221) or 1:5000 (FAP74) dilutions. Affinity-purified FAP221 antibody was used at a 1:500 dilution. Mouse monoclonal anti-IC2 antibody (King et. al., 1985) was used at 1:10,000 and rat monoclonal anti-HA (clone 3F10; Roche) was used at 1:2000.

Reverse transcriptase-PCR

The complete coding sequences for FAP46 and FAP54 were confirmed by reverse transcriptase-PCR performed as described previously (DiPetrillo and Smith, 2010). PCR primers were designed based on the predicted coding regions published in the *Chlamydomonas* genome database (http://genome.jgi-psf.org/Chlre3/Chlre3.home.html) or GreenGenie2 coding sequence prediction software (Kwan et al., 2009). Complete coding sequences were deposited into NCBI for FAP46 (accession number JF827824) and FAP54 (accession number JF827825).

Electron microscopy and analysis of swimming, flagellar beat frequency, and microtubule sliding

Electron microscopy and high-speed video microscopy were performed as previously described (DiPetrillo and Smith, 2011). Percent swimming, beat frequency, swimming velocity, and percent photoshock were measured manually or with ImageJ software (http://rsbweb.nih.gov/ij/) and statistical significance was determined using a Student's *t*-test. Beat frequency and swimming velocity data were graphed using Excel and proved to have a normal distribution (data not shown). Microtubule sliding velocities were measured as described previously (DiPetrillo and Smith, 2011). The ability of strains to photoaccumulate was assessed by placing a black plastic bag over a Petri dish filled with cells, leaving only a small edge of the dish exposed to light at an intensity of 14.2 µE (3.1 W/m^2). The cells were checked at 10-min intervals to see if photo-accumulation had occurred at the exposed edge of the dish.

Mass spectrometry

Silver-stained gel bands were excised and digested in gel with trypsin (proteomics grade; Sigma-Aldrich) at 37℃ overnight. Aliquots of tryptic peptides were first trapped on a Proxeon trap cartridge (100 µm×2 cm C18). Peptides were then eluted and sprayed from a custom-packed emitter (75 µm×25 cm C18) with a linear gradient from 100% solvent A (0.1% formic acid in 5% acetonitrile) to 35% solvent B (0.1% formic acid in acetonitrile) in 90 minutes at a flow rate of 300 nl/minute on a Proxeon Easy nanoLC system directly coupled to a Thermo LTQ Orbitrap Velos mass spectrometer. Data-dependent acquisitions were set up according to an experiment where full MS scans from 350–2000 Da were acquired in the Orbitrap at a resolution of 60,000 followed by 10 MS/MS scans acquired in the LTQ ion trap instrument. The raw data file was processed with Mascot Distiller (Matrixsciences, Ltd.) into peak lists and then searched against the *Chlamydomonas* taxonomy of the NCBInr database using the Mascot Search engine (Matrixsciences, Ltd.). Parent mass tolerances were set to 5 ppm and fragment mass tolerances were set to 0.5 Da. The variable modifications of acetyl (Protein N-term), pyro Glu for N-term Gln, propionamide of Cys, and oxidation of Met were used.

Sequence analysis and alignment

Predicted calmodulin-binding sites were identified by searching the Calmodulin Target Database (http://calcium.uhnres.utoronto.ca/ctdb/ctdb/sequence.html). Protein sequences were aligned with ClustalW2 (http://www.ebi.ac.uk/Tools/msa/clustalw2/) and the shaded alignment in supplementary material Fig. S2 was generated with Genedoc (available at http://sb.nrbsc.org/).

Acknowledgements

We thank Louisa Howard (Dartmouth College), and Gregory Hendricks and Lara Strittmatter (UMass Medical School) for technical assistance with electron microscopy. We also thank John

Leszyk and Scott Shaffer of the UMMS Proteomics and Mass Spectrometry Facility for MS. We are grateful to Winfield Sale (Emory University, Atlanta, GA) for generously providing anti-IC138 serum. E.F.S. and G.B.W. contributed equally to this work and are co-communicating senior authors.

Funding

This work was supported by National Institutes of Health [grant numbers GM030626 to G.B.W., GM066919 to E.F.S., 1F32GM093650 to J.M.B., 5T32HD007312 to J.M.B., 2T32GM008704 to C.G.D.]; a Copenhaver/Thomas Fellowship (to C.G.D.); and the Robert W. Booth Endowment (to G.B.W.). Deposited in PMC for release after 12 months.

Supplementary material available online at
http://jcs.biologists.org/lookup/suppl/doi:10.1242/jcs.107151/-/DC1

References

Adams, G. M., Huang, B., Piperno, G. and Luck, D. J. (1981). Central-pair microtubular complex of Chlamydomonas flagella: polypeptide composition as revealed by analysis of mutants. *J. Cell Biol.* **91**, 69-76.

Alvarez, L., Dai, L., Friedrich, B. M., Kashikar, N. D., Gregor, I., Pascal, R. and Kaupp, U. B. (2012). The rate of change in Ca(2+) concentration controls sperm chemotaxis. *J. Cell Biol.* **196**, 653-663.

Berthold, P., Schmitt, R. and Mages, W. (2002). An engineered Streptomyces hygroscopicus aph 7″ gene mediates dominant resistance against hygromycin B in Chlamydomonas reinhardtii. *Protist* **153**, 401-412.

Bessen, M., Fay, R. B. and Witman, G. B. (1980). Calcium control of waveform in isolated flagellar axonemes of Chlamydomonas. *J. Cell Biol.* **86**, 446-455.

DiPetrillo, C. G. and Smith, E. F. (2010). Pcdp1 is a central apparatus protein that binds Ca(2+)-calmodulin and regulates ciliary motility. *J. Cell Biol.* **189**, 601-612.

DiPetrillo, C. G. and Smith, E. F. (2011). The Pcdp1 complex coordinates the activity of dynein isoforms to produce wild-type ciliary motility. *Mol. Biol. Cell* **22**, 4527-4538.

Dutcher, S. K., Huang, B. and Luck, D. J. (1984). Genetic dissection of the central pair microtubules of the flagella of Chlamydomonas reinhardtii. *J. Cell Biol.* **98**, 229-236.

Elam, C. A., Wirschell, M., Yamamoto, R., Fox, L. A., York, K., Kamiya, R., Dutcher, S. K. and Sale, W. S. (2011). An axonemal PP2A B-subunit is required for PP2A localization and flagellar motility. *Cytoskeleton (Hoboken)* **68**, 363-372.

González-Ballester, D., de Montaigu, A., Galván, A. and Fernández, E. (2005). Restriction enzyme site-directed amplification PCR: a tool to identify regions flanking a marker DNA. *Anal. Biochem.* **340**, 330-335.

Gorman, D. S. and Levine, R. P. (1965). Cytochrome f and plastocyanin: their sequence in the photosynthetic electron transport chain of Chlamydomonas reinhardi. *Proc. Natl. Acad. Sci. USA* **54**, 1665-1669.

Hyams, J. S. and Borisy, G. G. (1978). Isolated flagellar apparatus of Chlamydomonas: characterization of forward swimming and alteration of waveform and reversal of motion by calcium ions in vitro. *J. Cell Sci.* **33**, 235-253.

Kamiya, R. and Witman, G. B. (1984). Submicromolar levels of calcium control the balance of beating between the two flagella in demembranated models of Chlamydomonas. *J. Cell Biol.* **98**, 97-107.

King, S. J. and Dutcher, S. K. (1997). Phosphoregulation of an inner dynein arm complex in Chlamydomonas reinhardtii is altered in phototactic mutant strains. *J. Cell Biol.* **136**, 177-191.

King, S. M., Otter, T. and Witman, G. B. (1985). Characterization of monoclonal antibodies against Chlamydomonas flagellar dyneins by high-resolution protein blotting. *Proc. Natl. Acad. Sci. USA* **82**, 4717-4721.

Kwan, A. L., Li, L., Kulp, D. C., Dutcher, S. K. and Stormo, G. D. (2009). Improving gene-finding in Chlamydomonas reinhardtii:GreenGenie2. *BMC Genomics* **10**, 210.

Lechtreck, K. F. and Witman, G. B. (2007). Chlamydomonas reinhardtii hydin is a central pair protein required for flagellar motility. *J. Cell Biol.* **176**, 473-482.

Lee, L., Campagna, D. R., Pinkus, J. L., Mulhern, H., Wyatt, T. A., Sisson, J. H., Pavlik, J. A., Pinkus, G. S. and Fleming, M. D. (2008). Primary ciliary dyskinesia in mice lacking the novel ciliary protein Pcdp1. *Mol. Cell. Biol.* **28**, 949-957.

Matsuo, T., Okamoto, K., Onai, K., Niwa, Y., Shimogawara, K. and Ishiura, M. (2008). A systematic forward genetic analysis identified components of the Chlamydomonas circadian system. *Genes Dev.* **22**, 918-930.

Mitchell, D. R. and Sale, W. S. (1999). Characterization of a Chlamydomonas insertional mutant that disrupts flagellar central pair microtubule-associated structures. *J. Cell Biol.* **144**, 293-304.

Mitchell, D. R. and Smith, B. (2009). Analysis of the central pair microtubule complex in Chlamydomonas reinhardtii. *Methods Cell Biol.* **92**, 197-213.

Pazour, G. J., Agrin, N., Leszyk, J. and Witman, G. B. (2005). Proteomic analysis of a eukaryotic cilium. *J. Cell Biol.* **170**, 103-113.

Pollock, S. V., Prout, D. L., Godfrey, A. C., Lemaire, S. D. and Moroney, J. V. (2004). The Chlamydomonas reinhardtii proteins Ccp1 and Ccp2 are required for long-term growth, but are not necessary for efficient photosynthesis, in a low-CO2 environment. *Plant Mol. Biol.* **56**, 125-132.

Rupp, G., O'Toole, E. and Porter, M. E. (2001). The Chlamydomonas PF6 locus encodes a large alanine/proline-rich polypeptide that is required for assembly of a central pair projection and regulates flagellar motility. *Mol. Biol. Cell* **12**, 739-751.

Stevens, D. R., Rochaix, J. D. and Purton, S. (1996). The bacterial phleomycin resistance gene ble as a dominant selectable marker in Chlamydomonas. *Mol. Gen. Genet.* **251**, 23-30.

VanderWaal, K. E., Yamamoto, R., Wakabayashi, K., Fox, L., Kamiya, R., Dutcher, S. K., Bayly, P. V., Sale, W. S. and Porter, M. E. (2011). bop5 Mutations reveal new roles for the IC138 phosphoprotein in the regulation of flagellar motility and asymmetric waveforms. *Mol. Biol. Cell* **22**, 2862-2874.

Wargo, M. J., Dymek, E. E. and Smith, E. F. (2005). Calmodulin and PF6 are components of a complex that localizes to the C1 microtubule of the flagellar central apparatus. *J. Cell Sci.* **118**, 4655-4665.

Wessel, D. and Flügge, U. I. (1984). A method for the quantitative recovery of protein in dilute solution in the presence of detergents and lipids. *Anal. Biochem.* **138**, 141-143.

Witman, G. B. (1986). Isolation of Chlamydomonas flagella and flagellar axonemes. *Methods Enzymol.* **134**, 280-290.

Witman, G. B. (1993). Chlamydomonas phototaxis. *Trends Cell Biol.* **3**, 403-408.

Witman, G. B., Plummer, J. and Sander, G. (1978). Chlamydomonas flagellar mutants lacking radial spokes and central tubules. Structure, composition, and function of specific axonemal components. *J. Cell Biol.* **76**, 729-747.